Fabrication and photoluminescence properties of Tb-doped nitrogen-rich silicon nitride films

Y.-T. An, C. Labbe, M. Morales, P. Marie, F. Gourbilleau

Fabrication and photoluminescence properties of Tb-doped nitrogen-rich silicon nitride films

Y.-T. An, C. Labbé*, M. Morales, P. Marie, and F. Gourbilleau

CIMAP, UMR CNRS/CEA/ENSICAEN/UCBN, 6 Boulevard Maréchal Juin, 14050 Caen Cedex 4, France

Keywords: magnetron sputtering, nitrogen-rich silicon nitride, Tb^{3+}, photoluminescence

*Corresponding author: e-mail christophe.labbe@ensicaen.fr

Terbium (Tb) doped nitrogen-rich silicon nitride thin films were prepared on [100] Si substrate by reactive magnetron co-sputtering in pure nitrogen atmosphere. The microstructure and optical properties of the films were investigated by means of ellipsometric spectroscopy (ES), atomic force microscopy (AFM), X-ray diffraction (XRD), Raman scattering and Fourier transform infrared (FTIR) spectroscopies as well as by photoluminescence (PL) experiments. A notable emission from Tb^{3+} ions was obtained for the as-deposited layer, while the maximum intensity was found from 600 °C-annealed sample. Deducing from PL excitation (PLE) analysis, a mechanism of excitation of Tb^{3+} ions was proposed: the band tail states of matrix play a minor role in the energy transfer process, while the host carriers across the optical gap acted as effective sensitizers for Tb^{3+} ions.

1 Introduction Si-rich silicon nitride (SRSN) material has received great interest in the last decades. Its lower band gap and larger density of trap states are in agreement with the need of low injection voltages for applications in light emitting diode (LED) devices [1, 2]. Moreover, the Si excess can form Si nano-clusters which contributes to visible photoluminescence but can plays sensitizing role towards rare earth (RE) ions too [3, 4].

In contrast to SRSN, nitrogen-rich silicon nitride (NRSN) films are also considered as a promising candidate for LED devices, as they show better interface properties when used in silicon-based metal-insulator-semiconductor devices and have better negative charge ability and stability [5]. The NRSN layers have been deposited by many groups using a conventional approach of plasma enhanced chemical vapor deposition (PECVD) [5-7]. In this case, the film composition was tuned through the SiH_4/NH_3 ratio. Such a film presents numerous band tail states and small band gap [8] which can play the role of sensitizer for RE ions. Tb^{3+} ions offer an interesting green emission at a 543 nm wavelength for future Si-based LED devices. Yuan et al. [7] have evidenced an efficient energy transfer from matrix to Tb^{3+} ions in Tb-implanted silicon nitride layer fabricated by PECVD. The same process has been demonstrated in Tb-doped silicon oxynitride matrix [9].

In this study, we deposited films by means of reactive magnetron sputtering of a Si target toped with Tb_4O_7 chips in pure N_2 plasma. The sputtered Si atoms react with N_2 in the plasma to allow the growing of a NRSN matrix. The structural properties of the layers were characterized by various methods such as X-ray diffraction (XRD), ellipsometric (ES), and Raman scattering spectroscopies. Room temperature PL as well as dynamic PL behavior was investigated as a function of annealing temperature (T_A). The energy transfer mechanism was also analyzed by means of PL excitation (PLE) experiments.

2 Experimental details The films were grown on p-type 250 μm-thick [001]-Si single crystalline wafers by reactive magnetron co-sputtering of a pure Si target topped with a given number of Tb_4O_7 chips under pure nitrogen plasma at a pressure of 23 μbar. The substrate temperature and RF power density were fixed at 200 °C and 5 $W \cdot cm^{-2}$, respectively. The annealing of the deposited thin layers were performed in a conventional furnace in a 500-1100 °C range for 1 h in a dry nitrogen flow.

The refractive index and the thickness were deduced from ES with an incident light ranging from 1.5-4.5 eV by using a Jobin-Yvon ellipsometer. The sample structure was studied using XRD and Raman spectroscopy. The XRD measurements experiments were performed using a Philips Xpert NPD Pro diffractometer mounted with a point scintillation detector in the θ-2θ configuration. Raman spectra were measured with 532 nm continuous waver laser by means of Dispersive Horiba Yvon Raman spectrometer equipped with confocal microprobe and CCD camera. For this latter, the experiments were performed on films deposited on fused silica substrates instead of silicon ones. The infrared absorption properties were investigated by means of a Nicolet Nexus Fourier Transmission Infrared (FTIR) spectroscopy in 500-4000 cm^{-1} range. The PL emission and PLE measurements were carried out using a 450 W xenon arc lamp as excitation source at room temperature with help of Jobin-Yvon Fluorolog spectrometer. The lifetime was obtained by means of an optical parametric oscillator with a pulse of 5 ns at full width at half maximum and a repetition rate of 10 Hz for a 244 nm wavelength excitation. The spot diameter was 500µm with an average energy of 15 mJ.

3 Results and discussion

3.1 Film microstructure The refractive index was investigated by ellipsometric spectroscopy and fitted by an effective medium approximation model. For the as-deposited sample, the refractive index was 1.71 at 1.95 eV. This value was quite lower than that of stoichiometric Si_3N_4 (about 2.04) at this energy [10], which is the signature of the growth of Nitrogen-rich-Silicon Nitride film (NRSN) [8]. To be sure that this lower refractive index is not the result of an important roughness resulting from the reactive deposition process [11], atomic force microscopy observations (image not shown here) were performed. The layer surface presents root mean square roughness values less than 1 nm attesting that the produced layer is the expected NRSN film.

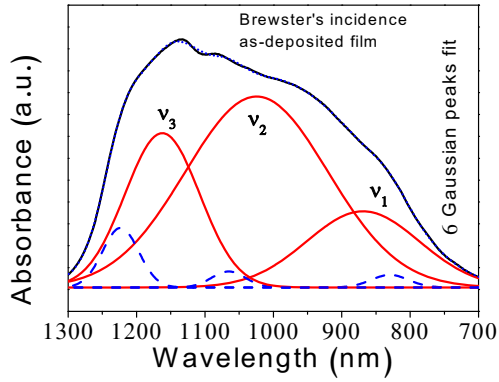

Figure 1 FTIR spectrum of as-deposited film recorded at Brewster angle (65°).

Figure 1 depicts a typical FTIR spectrum recorded at Brewster incidence (65°) for the as grown film. This spectrum was fitted with six Gaussian curves centered at 825, 860, 1020, 1070, 1161 and 1225 cm^{-1}, respectively. The main absorption peaks located at 860 (TO), 1020 (TO), and 1161 (LO) cm^{-1} were attributed to Si-N asymmetric stretching mode named as ν_1, ν_2 and ν_3, respectively. It is reported that the blueshift of the Si-N stretch mode was agreed with the increase of nitrogen content in silicon nitride film [12-14]. Bustaret et al. [12] reported in addition the main Si-N bonds at 850 cm^{-1}, a strong shoulder in the 970-1010 cm^{-1} range grown with nitrogen content. Our sample had a much higher ν_2 TO Si-N position at 1020 cm^{-1} which is evidence that we have grown a NRSN film. The other three peaks, in Fig. 1, located at 1225 cm^{-1} (LO_3), 1070 cm^{-1} (TO_3), and 825 cm^{-1} (TO_2 and LO_2) in blue dashed line are all assigned to Si-O bonds. The presence of oxygen atoms in the film is attributed to the sputtering of the Tb_4O_7 chips used.

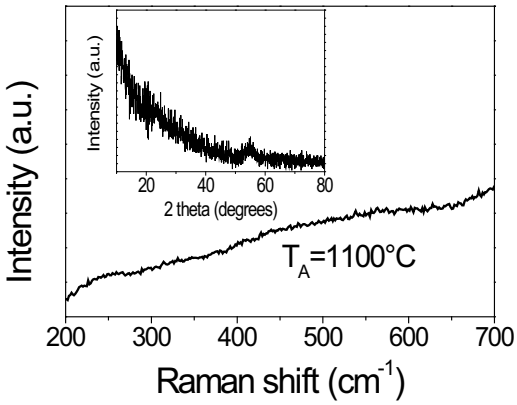

Figure 2 Raman spectrum on fused silica sample annealed at 1100 °C. The inset showed XRD pattern of Tb-doped film annealed at 1100 °C.

The Raman analysis was performed on an 1100 °C-annealed film grown on fused silica substrate (Fig. 2). No peak appears at 520 cm^{-1} which means that no crystallized Si grains are present in the layer. This is confirmed by the XRD experiments (inset of Fig. 2) which do not show any peak issue from the diffraction on Si planes. The presence of a peak at 55° is attributed to the substrate. These microstructural investigations attest the amorphous nature of the annealed layer even after a high temperature annealing process [15, 16].

3.2 PL spectroscopy

The PL behavior of the films was explored for the different annealing temperature using an excitation wavelength of 325 nm (Fig. 3). Four emission peaks in the 480-640 nm range and a broad band emission with lower intensity compared to the Tb^{3+} PL intensity have been detected. Such broad emission band which is usually attributed to the band tails states [8] is expanded to 340 nm due to the composition in our film.

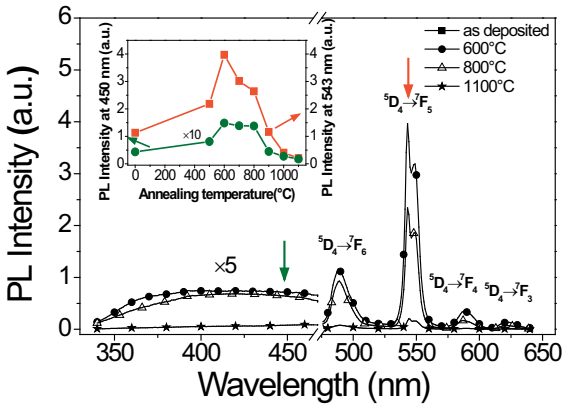

Figure 3 PL spectra excited at 325 nm for different annealing temperature. Inset is PL intensities at 543 nm (Tb^{3+}) and 450 nm (band tail states) as a function of the annealing temperature.

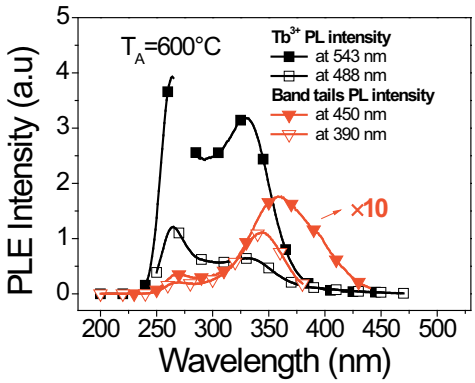

Figure 4 PLE spectra of 600 °C-annealing sample monitored at 543 nm, 488 nm (Tb^{3+} related) and 450 nm and 390 nm (band tails).

The PL intensity increases with T_A to reach the maximum in the 600-800 °C range and then decreases for highest annealing temperatures. Concerning the four peaks are centered at about 488, 543, 590, and 621 nm, they correspond to the intra-4f $^5D_4 \rightarrow ^7F_6$, $^5D_4 \rightarrow ^7F_5$, $^5D_4 \rightarrow ^7F_4$ and $^5D_4 \rightarrow ^7F_3$ transitions of Tb^{3+} ions, respectively. One can notice the presence of a significant emission from Tb^{3+} ions even for the as-deposited sample. The maximum emission of Tb^{3+} is achieved after an annealing treatment at 600 °C following by a decrease for higher T_A (inset of Fig. 3). Band tails and Tb ions emissions present the same evolution with the annealing temperature. The behavior for the low T_A range is explained by the fact that the annealing treatment decreases the nonradiative recombination rates and consequently increases the PL intensity of both host matrix and Tb^{3+} ions [17]. Annealing above 600 °C favors the Tb agglomeration, which, consequently, quench the Tb emission [18]. In the same time, no increase of the band tails emission is observed at high temperature. This annealing treatment in a nitrogen flow should favor the rearrangement of the matrix leading to the recovering of the radiative defects and thus can explain the quenching observed in 350-460 range. It is worth to note that the Tb^{3+} luminescence decay at 1000 °C (not shown here) is characterized by a stretch exponential decay with a life time of almost 600 µs at 543 nm. Such a value agrees with those achieved in Tb-doped films annealed at this temperature [9].

The Fig. 4 depicts the PLE spectra collected for the broad band emission at 390 or 450 nm and for the Tb-emission wavelengths at 488 and 543 nm for sample annealed at 600 °C. The Tb^{3+} PL showed an overall increase with the decreasing of excitation wavelength (from 480 to 265 nm). Two clear peaks were observed in the Tb-PLE spectra, locating at around 265 and 330 nm, respectively. The PLE spectra reflect the absorption of the different elements constituting the matrix. In fact, the typical absorption spectrum for rare earth in the absence of energy sensitization process from host matrix should appear as a set of discrete peaks, corresponding to the inhomogeneous broadening of Tb ions [19]. Our Tb-PLE spectra do not reveal any well-defined peaks. This implies that Tb^{3+} ions are not resonantly excited in the UV range (250-400 nm) but underlines an energy transfer coming from other elements of the matrix to Tb^{3+} ions.

The broad band PLE spectra of the band tails (red triangle) showed the same peak position at 265 nm. This result was the same as that of Tb with detection at 488 nm in black line. Therefore, the PLE spectra of both matrix and Tb appeared to have a similar contribution from a strong peak at 265 nm (4.7 eV), which suggests a presence of high efficient energy transition. In other words, the major contribution for the Tb-PL comes from this transition that could arise from the N pπ lone pair states near the valence band in NRSN films [20].

The film studied in this work was considered to hold ~4.7 eV optical Tauc gap according to our refractive index, which agreed well with the previous reported values of silicon nitride [2, 8]. Therefore, in the Tb-PLE spectra the peak at 4.7 eV should come from the carriers across the optical gap into the extended states-carriers that could be captured directly by Tb^{3+}-related states [9]. As a consequence, the carriers in the extended N pπ states played the main sensitizer role of Tb^{3+} ions. The PLE roll off at high photon energies excitation can be attributed to the reducing of the energy transfer efficiency due to the carrier thermalization into efficient nonradiative trap states [21].

The PLE peak of Tb ions at 330 nm observed in the case of Tb ions is attributed to the band tail absorption in the NRSN matrix [7]. The two wavelengths detection at 390 nm and 450 nm described two different PLE peaks centered at 340 and 360 nm, respectively. This shifting behavior with the detecting wavelength is feature of states density due to the filling of the band tail states.

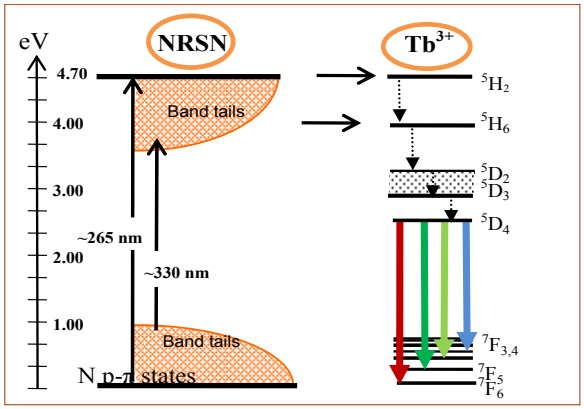

Figure 5 Schematic band diagram of the Tb-NRSN film with a mechanism proposed to explain the PL in the NRSN film.

In the light of these results, a qualitative model is proposed here to explain the optical behavior observed in our films, as shown in the scheme (Fig. 5). There are two main energy transfer mechanisms identified between matrix and Tb^{3+} ions. When excited around 265 nm, corresponding to the gap at 4.7 eV, the carriers mediated in matrix are excited and an energy transfer to the Tb^{3+} excited states $^5H_2$ occurs. It is followed by the non-radiative relaxation from states $^5H_2$ to $^5D_4$ and then to the ground states with four peak emissions. When excited energy is lower than the gap, carriers trapped in the band tails states can transfer weak energy to Tb^{3+} ions.

4 Conclusions The films were deposited by sputtering method and attested as NRSN by low refractive index, the absence of crystalline grains and the blueshift and broaden shoulder for Si-N bonds in FTIR spectroscopy. The strong Tb^{3+} emission was obtained by optimizing the annealing condition. On the basis of PLE spectra, two processes of energy transfer to Tb^{3+} may exist: band tail states, carrier mediated. Furthermore, the carrier mediated was considered to play a main role in obtaining high Tb emission and band tail states act a supporting role.

Acknowledgements The authors would like to thank Dr. Sophie Boudin from CRISMAT lab with the measurement of PL and PLE spectra. This work is supported by the contract CEA/DSM/HOFELI and the program of Chinese Scholarship Council (CSC).

References

[1] L. Dal Negro, J. H. Yi, and L. C. Kimerling, Appl. Phys. Lett. **88**, 233109 (2006).
[2] M. Wang, J. Huang, and L. Pavesi, J. Appl. Phys. **104**, 083505 (2008).
[3] R. P. Nalini, L. Khomenkova, and F. Gourbilleau, Nano-scale Res. Lett. **7**, 124 (2012)
[4] E. Steveler, H. Rinnert, and M. Vergnat, Appl. Phys. Lett. **97**, 221902 (2010).
[5] Y. L. Ren, K. J. Weber, and N. M. Nursam, Appl. Phys. Lett. **98**, 122909 (2011).
[6] L. Wang, H. S. Reehal, and A. del Prao, Semicond. Sci. Technol. **18**, 633 (2003).
[7] Z. Z. Yuan, D. S. Li, and D. R. Yang, J. Appl. Phys. **100**, 083106 (2006).
[8] J. Kistner, X. Chen, and J. H. Werner, J. Appl. Phys. **110**, 023520 (2011).
[9] H. Jeong, S. Y. Seo, and J. H. Shin, Appl. Phys. Lett. **88**, 161910 (2006).
[10] T. Baak, Appl. Optics **21**, 1069 (1982).
[11] G. Xu, P. Jin, and K. Yoshimura, Thin Solid Films **425**, 196 (2007).
[12] E. Bustarret, M. Besouda, and S. C. Gujrthi, Phys. Rev. B **38**, 8171 (1988).
[13] C. Sénémaud, A. Gheorghiu, and S. Gujrathi, J. Non-Cryst. Solids **164**, 1073 (1993).
[14] K.-C. Lin and S.-C. Lee, J. Appl. Phys. **72**, 5474 (1992).
[15] M. Molinari, J. Appl. Phys. **101**, 123532 (2007).
[16] G. Scardera, G. Scardera, and M. A. Green, J. Appl. Phys. **104**, 104310 (2008).
[17] H. Kato, A. Masuzawa, T. Noma, K. S. Seol, and Y. Ohki, J. Phys.: Condens. Matter **13**, 6541 (2001).
[18] A. Polman, D. C. Jacobson, and J. M. Poate, J. Appl. Phys. **70**, 3778 (1991).
[19] D. B. He, C. L. Yu, and L. L. Hu, J. Rare Earth **29**, 48 (2011).
[20] W. L. Warren, J. Kanicki, and P. M. Lenahan, Appl. Phys. Lett. **59**, 1699 (1991).
[21] R. A. Street, Adv. Phys. **25**, 397 (1976).